Ceramics International 47 (2021) 1855–1864

Contents lists available at ScienceDirect

Ceramics International

journal homepage: www.elsevier.com/locate/ceramint

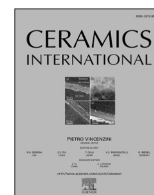

Role of oxygen in surface kinetics of SiO_2 growth on single crystal SiC at elevated temperatures

Yongjie Zhang [a,1], Shaoxiang Liang [a,1], Yi Zhang [a,b], Rulin Li [a], Zhidong Fang [a], Shuai Wang [a], Hui Deng [a,*]

[a] Department of Mechanical and Energy Engineering, Southern University of Science and Technology, Shenzhen, Guangdong, 518055, PR China
[b] Engineering, Faculty of Science, University of East Anglia, Norwich Research Park, Norwich, NR4 7TJ, UK

ARTICLE INFO

Keywords:
Single crystal SiC
Thermal oxidation
Thermal CVD
Oxygen concentration
Surface kinetics

ABSTRACT

Understanding surface kinetics of SiO_2 growth on single crystal SiC at elevated temperatures is crucial to fabricate high-performance SiC-based devices. However, the role of oxygen in the evolution mechanism of SiC surface at atomic scale has not been comprehensively elaborated. Here, we reveal the manipulation effect of oxygen on the competitive growth of thermal oxidation SiO_2 (TO-SiO_2) and thermal chemical vapor deposition SiO_2 (TCVD-SiO_2) on the 4H-SiC substrate at 1500 °C. TO-SiO_2 is formed by the thermal oxidation of SiC, in which the substrate undergoes layer-by-layer oxidation, resulting in an atomically flat SiC/TO-SiO_2 interface. TCVD-SiO_2 growth includes the sublimation of Si atoms, the reaction between sublimated Si atoms and reactive oxygen, and the adsorption of gaseous Si_xO_y species. A relatively high sublimation rate of Si atoms at SiC atomic steps causes the transverse evolution of the nucleation sites, leading to the formation of nonuniform micron-sized pits at the SiC/TCVD-SiO_2 interface. The low oxygen concentration favors TCVD-SiO_2 growth, whose crystal quality is much better than that of TO-SiO_2 due to the high surface mobility in the thermal CVD process. We further achieve the epitaxial growth of graphene on 4H-SiC in an almost oxygen-free reaction atmosphere. Additionally, ReaxFF reactive molecular dynamic simulation results illustrate that the decrease in oxygen concentration can promote the growth kinetics of SiO_2 on single crystal SiC from being dominated by thermal oxidation to being dominated by thermal CVD.

1. Introduction

As the most attractive third-generation semiconductor material, single crystal SiC possesses many excellent properties such as a wide band gap, a high breakdown electric field, and high thermal, mechanical, and chemical stability [1–4]. Thus, SiC is a promising material for high-temperature, high-power, and high-frequency electronic devices [4–6], and various surface treatment technologies have been explored to promote its applications. Typically, SiC can be thermally oxidized to form an insulating oxide layer, which is indispensable for making SiC-based devices, for instance, SiC metal-oxide-semiconductor field effect transistors (MOSFETs) [7,8]. The thermal oxidation kinetics of SiC with different crystal orientations, performed in 1 atm dry oxygen and in the temperature range of 950–1150 °C, has been well demonstrated by the modified Deal-Grove model [9]. The above conventional thermal oxidation of SiC can inevitably cause significant amount of both interface defects and near-interface traps, thus deteriorating the performance (especially the inversion channel mobility) and the reliability of SiC-based devices [10–12]. Although it has been reported that increasing oxidation temperature can improve the characteristics of SiC-based devices by enhancing the oxidation process of C atoms to suppress the interface trap density to a relatively low level [10,12], few studies have focused on the oxidation kinetics of SiC at atomic scale at a temperature higher than the conventional thermal oxidation temperature of SiC. On the other hand, with the emergence of graphene fabricated by the mechanical exfoliation method [13], many other approaches have been presented to produce graphene with large domain size, high quality, and uniform layers; among these methods, the epitaxial growth of graphene on the SiC substrate is considered to be the most promising method to promote the application process of graphene and SiC in the field of electronics [14–17]. The mechanism of the SiC-based epitaxial growth method lies in the sublimation of Si atoms

* Corresponding author.
E-mail address: dengh@sustech.edu.cn (H. Deng).
[1] These two authors contributed equally to this work.

https://doi.org/10.1016/j.ceramint.2020.09.014
Received 5 August 2020; Received in revised form 26 August 2020; Accepted 1 September 2020
Available online 2 September 2020
0272-8842/© 2020 Elsevier Ltd and Techna Group S.r.l. All rights reserved.

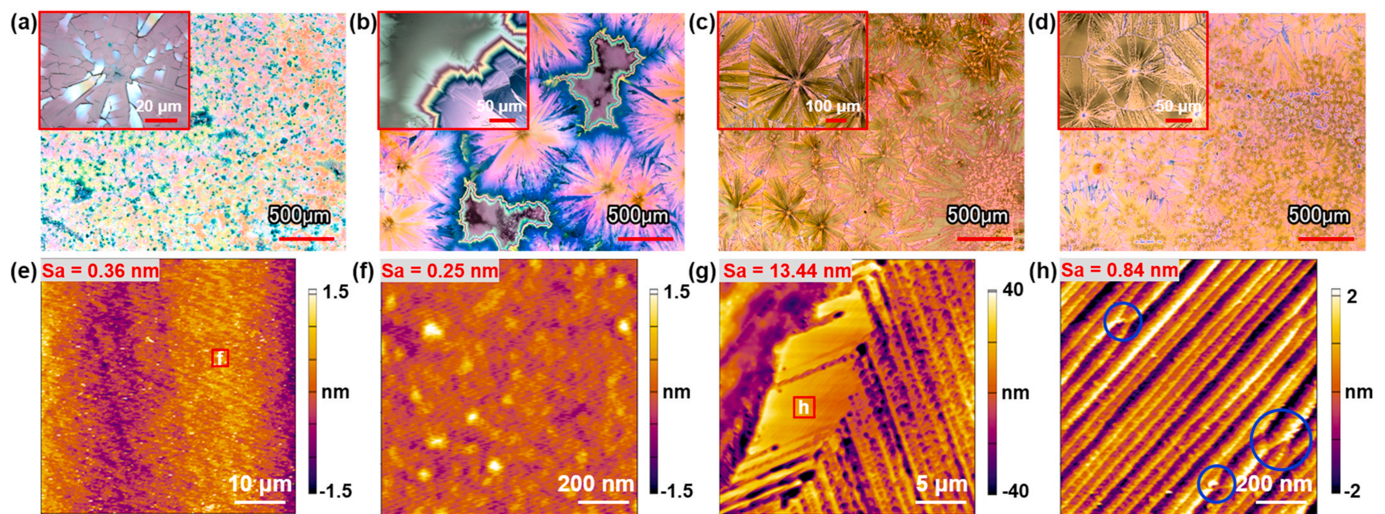

Fig. 1. Morphology of the 4H-SiC heated at 1500 °C and different pressures for 10 min. (a)–(d) LSCM images at 1 atm (adequate oxygen concentration), 100 Pa (moderate oxygen concentration), 10 Pa (slight oxygen concentration), and 0.1 Pa (very low oxygen concentration), respectively. The inserts are the corresponding high-resolution LSCM images. (e)–(h) AFM images of the sample in (b): (e) and (f) thermal oxidation domain, (g) and (h) thermal CVD domain.

and the rearrangement of C atoms at elevated temperatures (~1500 °C) and under high vacuum conditions.

In general, sufficient oxygen is necessary to conduct the thermal oxidation of SiC, while oxygen should be maximally isolated to grow graphene on the SiC substrate. Thus, oxygen is believed to have a substantial influence on the surface kinetics of SiC at elevated temperatures. However, an atomic-level investigation of the surface kinetics of single crystal SiC under elevated temperatures and different oxygen concentrations conditions, which is the key to fabricate high-performance SiC-based devices, is lacking.

In this work, we reveal the role of oxygen in the surface kinetics of SiO_2 growth on single crystal SiC at elevated temperatures by experiments and ReaxFF reactive molecular dynamics simulation. Through the oxidation experiments of SiC at different oxygen concentrations and temperatures, we find a competitive growth between thermal oxidation SiO_2 (TO-SiO_2) and thermal chemical vapor deposition SiO_2 (TCVD-SiO_2) on SiC, and the oxidation results show that the low oxygen concentration favors the formation of TCVD-SiO_2, which presents the radial-structured patterns. The morphologies and atomic bonding conditions of the two oxide indicate that the crystal quality of TCVD-SiO_2 is much better than that of TO-SiO_2. We demonstrate the layer-by-layer oxidation mechanism for TO-SiO_2 growth and the SiC atomic steps transverse evolution mechanism for TCVD-SiO_2 growth. In addition, the epitaxial growth of graphene on SiC is achieved in an almost oxygen-free atmosphere. Moreover, the simulation results illustrate that the decrease in oxygen concentration can promote the growth kinetics of SiO_2 on SiC from being dominated by thermal oxidation to being dominated by thermal CVD.

2. Materials and methods

2.1. Sample preparation

High purity semi-insulating 4H-SiC (0001) substrates (on-axis) purchased from SICC Materials Co., Ltd. Were used in this study. Before the experiments, the SiC wafers were cut into square pieces with a side length of 10 cm using a dicing system (Veeco Optium ADS-800). To remove various kinds of contamination on the SiC square pieces, all samples were cleaned in sequence by SC_1 ($NH_4OH/H_2O_2/H_2O$), SC_2 ($HCl/H_2O_2/H_2O$), and BOE ($HF/NH_4F/H_2O$) for 10 min, followed by being rinsed in ultrapure water for 5 min. Finally, these SiC square pieces were dried with nitrogen. The SiC surfaces (0001) after these processes are defined as the as-received surfaces in this study.

2.2. Experimental details

2.2.1. Oxidation of SiC

For the oxidation experiments of SiC, the SiC samples with the Si-face (0001) up were placed in a corundum crucible, and then heated in a tube furnace (GSL-1700X, Heifei Kejing Materials Technology Co., Ltd). The adopted heating element was a silicon-molybdenum rod, and the temperature was controlled by a temperature controller (YD518P). The heating rate was set to 3 °C/min, while the cooling rate was constant at 5 °C/min. A molecular pump (FJ-80, Kyky Technology Co., Ltd) was used to achieve different vacuum degrees, which were measured by a multi-gauge vacuum meter (ZDF-11A2, Kyky Technology Co., Ltd). Four furnace pressures were applied, 1 atm, 100 Pa, 10 Pa, and 0.1 Pa, representing adequate, moderate, slight, and very low oxygen concentrations, respectively.

2.2.2. Growth of graphene

The epitaxial growth of graphene on the SiC substrate was completed in an ultrahigh temperature heat treatment equipment (SR1800G, Thermo Riko Co., Ltd). The SiC samples with the Si-face (0001) up were placed in a graphite holder. The heating process was achieved by an infrared lamp (2 kW), and the heating rate was set to 300 °C/min. The pressure in the heating chamber was about 1.0×10^{-3} Pa.

2.3. Characterizations

Laser scanning confocal microscopy (LSCM) images were obtained by a KEYENCE VK-X1000. Atomic force microscope (AFM) images in Fig. 1 were acquired using an Asylum Research MFP-3D-Stand Alone in tapping mode, and AFM images in Fig. 6 were obtained by a BRUKER Dimension Edge in tapping mode. Energy dispersive X-ray spectroscopy (EDS) mapping results and Kikuchi diffraction patterns were acquired on a scanning electron microscopy (Zesis Merlin, accelerator voltage: 10 kV). X-ray photoelectron spectroscopy (XPS) results were obtained by a PHI 5000 VersaProbe III spectrometer with a monochromatic Al *Kα* X-ray source. The vacuum was maintained at or below 10^{-9} Torr for data acquisition. For each XPS analysis, the size of the measured area was set to 100 μm × 1400 μm. Data analyses were carried out by XPS PEAK 41 software. During element curve fitting, a 'Shirley' background subtraction method and a 'Lorentzian-Gaussian' function with a ratio of 20% (0:

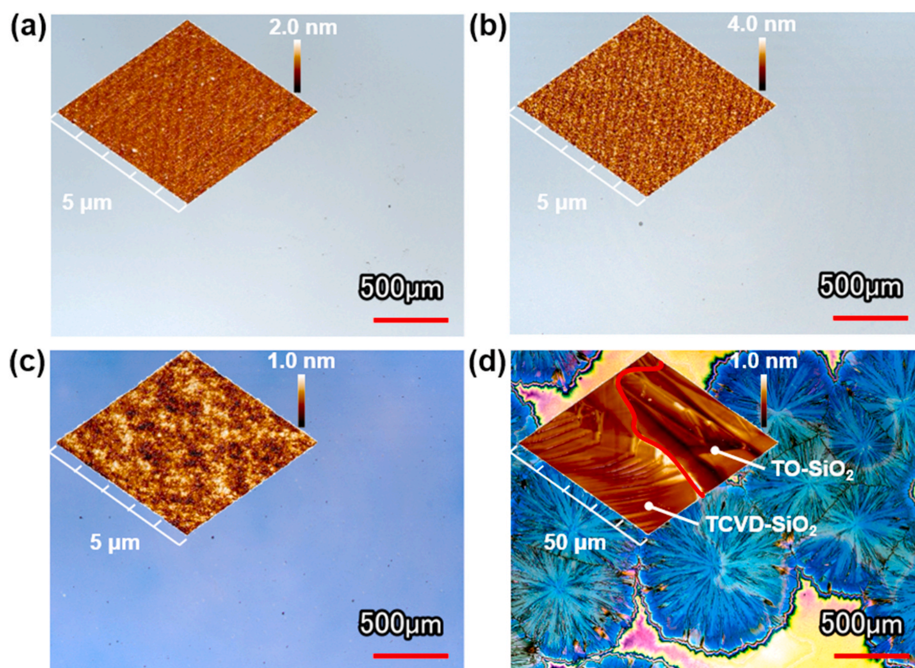

Fig. 2. Morphology of the 4H-SiC heated at 100 Pa and different temperatures for 10 min. (a)–(d) LSCM images at 900 °C, 1100 °C, 1300 °C, and 1500 °C, respectively. The inserted AFM images show the corresponding 3D morphologies.

Gaussian, 100: Lorentzian) were chosen. Transmission electron microscopy (TEM) images were obtained using a JEM 3200FS under 300 kV. Raman spectra were measured on a confocal Raman spectroscopy (HORIBA LabRAM HR Evolution) equipped with a laser with a wavelength of 532 nm.

2.4. ReaxFF reactive molecular dynamics simulation

All simulations were conducted using the Large-scale Atomic/Molecular Massively Parallel Simulator (LAMMPS) simulation package. The simulation results were visualized by an open visualization tool (Visual Molecular Dynamics, VMD). The size of the Setup A periodic cell was $61.61 \times 100.85 \times 81.70$ Å, containing 18360 O atoms, and 20400 Si and C atoms, and the periodic cell of Setup B was enlarged to $61.61 \times 300 \times 81.70$ Å but contained the same number of O, Si, and C atoms. The temperatures in the two setups were set to 1800 K. For the setup in Fig. S2, except for the temperature changing from 1200 K to 2700 K with an interval of 300 K, other parameters were consistent with Setup A.

3. Results and discussion

3.1. Competitive growth of TO-SiO_2 and TCVD-SiO_2

Fig. 1 shows the morphology of the 4H-SiC processed at 1500 °C and different pressures (oxygen concentrations) for 10 min. In Fig. 1(a), SiO_2 blocks were formed on SiC at 1 atm, and many microcracks distributed radially were observed. Under these conditions, the thermal oxidation reaction of SiC ($2SiC + 3O_2 \rightarrow 2SiO_2 + 2CO$) occurred rapidly, resulting in the formation of a thick oxide layer. This kind of SiO_2 is directly formed by the thermal oxidation of SiC, and is denoted as TO-SiO_2 in the remainder of this paper. When the pressure was reduced to 100 Pa (Fig. 1(b)), the effect of thermal oxidation was weakened to some extent, and Si atoms readily eliminated the restriction of the thermal oxide layer and sublimated into the atmosphere inside the furnace [9,16]. Once the sublimated Si atoms reacted with the active oxygen, gaseous SiO_2 was formed and could be adsorbed by the SiC substrate ultimately ($SiC \rightarrow Si\uparrow + C$, $Si + O_2 \rightarrow SiO_2$). This kind of SiO_2 is generated by the thermal CVD process, and is denoted as TCVD-SiO_2 hereafter. Fig. 1(b) shows the radial-structured patterns of TCVD-SiO_2. Studies have reported the dendritic shapes of thin film materials during the CVD process, for example, graphene, hexagonal boron nitride (h-BN), and transition metal dichalcogenides (TMDs) [18–21]. Many efforts have been made to illustrate the underlying atomic mechanism in terms of the oxygen effect [18], hydrogen etching [22], edge-energy equilibrium [23], classical Wulff structure [24], and phase-field approach [25]. In our study, the formation of radial SiO_2 patterns is determined by the oxygen concentration.

In Fig. 1(b), TCVD-SiO_2 growth was dominant over TO-SiO_2 growth, resulting in several thermal oxidation domains distributed among many radial-structured patterns. If the pressure was further reduced to 10 Pa (Fig. 1(c)), TCVD-SiO_2 growth was further enhanced relatively, as no thermal oxidation domains were found on the surface. Additionally, there is an obvious contrast in the density and size of radial-structured patterns in Fig. 1(b)-1(d). It seems that with a decrease in oxygen concentration, the density of radial-structured patterns dramatically increases, while the size of the patterns significantly decreases. Thus, oxygen is considered to play an important role in manipulating the surface kinetics of SiO_2 growth on SiC.

According to Fig. 1(e) and (f), the typical characteristics of thermally oxidized SiC such as the formation of SiO_2 nanoparticles and the flat oxidized surface were observed [26,27]. Fig. 1(g) shows the typical microtopography of a branch of a radial-structured pattern in Fig. 1(b); on the edge of this pattern, the atomic steps of SiO_2 are clearly detected (Fig. 1(h)). Furthermore, some dislocation-like features are present among the steps, as marked by the blue circles in Fig. 1(h). Hence, it can be concluded that the thermal CVD domains are made up of monocrystalline or polycrystalline SiO_2, and the generation of dislocation-like features is attributed to the motion of atoms under the action of elevated temperatures, stress and other factors during the thermal CVD process [28–30]. In contrast, the thermal oxidation domains are comprised of amorphous SiO_2 [31]. Thus, it may be deduced that the crystal quality of TCVD-SiO_2 is better than that of TO-SiO_2, and our speculation is verified in section 3.2.

As previously mentioned, the ability of oxygen to manipulate the competitive growth of TO-SiO_2 and TCVD-SiO_2 is based on the elevated

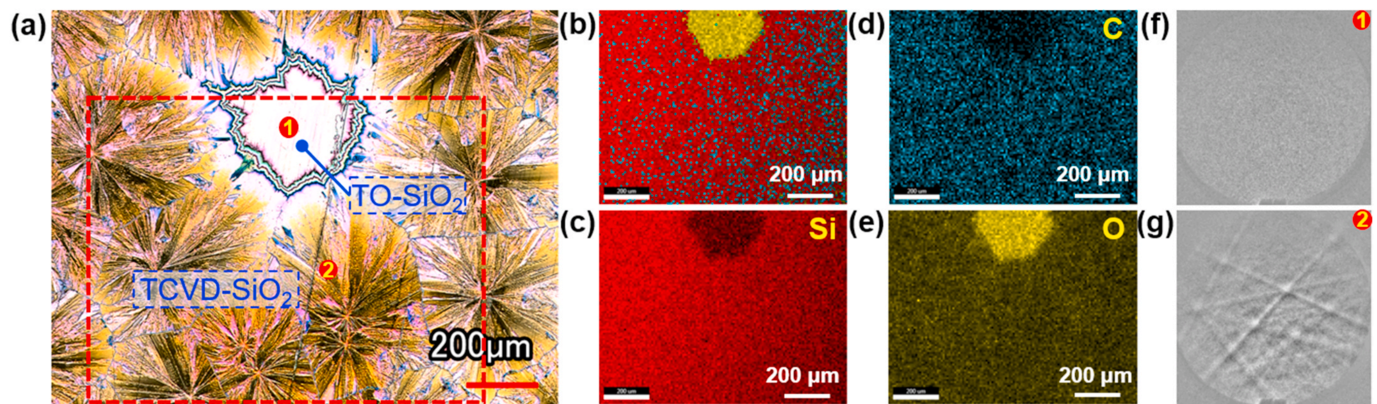

Fig. 3. EDS elemental mapping results and Kikuchi diffraction patterns of the 4H-SiC heated at 1500 °C and 100 Pa for 10 min. (a) LSCM image of the heated 4H-SiC. (b)–(e) EDS mapping results of the red dotted box in (a): (b) the mapping result of all elements (Si, C, and O), (c)–(e) the mapping results of Si, C, and O elements, respectively. (f) and (g) Kikuchi diffraction patterns of position 1 and position 2 in (a), respectively. (For interpretation of the references to colour in this figure legend, the reader is referred to the Web version of this article.)

temperature conditions. We verified the importance of temperature in this process by heating SiC at 100 Pa with different temperatures (900 °C, 1100 °C, 1300 °C, and 1500 °C) for 10 min, as shown in Fig. 2. According to the modified Deal-Grove model for the thermal oxidation of SiC, once SiC is heated above 900 °C in an oxygen-containing reaction system, an oxide layer is formed on its surface, accompanied by the diffusion of CO from the SiO_2/SiC interface [9]. In Fig. 2(a), almost no apparent oxidation results can be distinguished owing to the short reaction time and the relatively low temperature. The atomic steps of the original polished SiC still can be detected by AFM, according to the inserted 3D morphology image. At 1100 °C in Fig. 2(b), SiO_2 began to grow along the steps of the SiC substrate. The corresponding insert indicates that the surface is still atomically flat with visible steps. However, a noticeable layer of TO-SiO_2 was formed on the SiC substrate when the temperature increased to 1300 °C (Fig. 2(c)), and the typical features as SiC underwent thermal oxidation are illustrated in the relevant AFM image. Moreover, the nucleation sites of TCVD-SiO_2 appeared on the substrate surface, which are depicted as the black pits in Fig. 2(c). Nevertheless, the growth of TCVD-SiO_2 was extremely weak due to the extraordinarily low sublimation rate of Si atoms at 1300 °C. Therefore, it is reasonable that no radial SiO_2 patterns were formed. Predictably, once the temperature reached 1500 °C and the Si atoms sublimated from SiC quickly, radial-structured patterns attributed to the growth of TCVD-SiO_2 emerged, as shown in Fig. 2(d). The inserted AFM image shows the boundary between TCVD-SiO_2 and TO-SiO_2. The above results show that only when the temperature reaches 1500 °C, which can accelerate the sublimation process of Si atoms, the radial-structured patterns of TCVD-SiO_2 can be formed. Thus, it is concluded that the elevated temperature is an essential prerequisite for the manipulation effect of oxygen on the growth modes of SiO_2 on SiC.

3.2. Difference in crystal quality between TO-SiO_2 and TCVD-SiO_2

The different growth processes of TO-SiO_2 and TCVD-SiO_2 lead to significant differences in the element distributions and the atomic bonding conditions in the thermal oxidation domain and the thermal CVD domain. Fig. 3(b)-3(e) show the EDS mapping results of the red dotted area marked in Fig. 3(a), which includes both the aforementioned domains. It is clear that the thermal oxidation domain contains more O element and fewer C and Si elements than the thermal CVD domain. The difference in element distributions is due to the difference in oxidation extents in these two domains. Clearly, TO-SiO_2 is always formed prior to TCVD-SiO_2, because the thermal oxidation temperature of SiC is lower than the sublimation temperature of Si atoms from SiC. Consequently, the thickness of the TO-SiO_2 film is greater than that of the TCVD-SiO_2 film, which is also verified in Fig. 5(e) and (h). The thicker TO-SiO_2 layer gives rise to the higher oxygen content in the thermal oxidation domains, and the stronger atomic signals of C and Si elements in the thermal CVD domains originate from the SiC substrate. Kikuchi diffraction patterns were used to evaluate the crystal state of TO-SiO_2 and TCVD-SiO_2 [32,33]. As shown in Fig. 3(f) and (g), a clear Kikuchi diffraction pattern of SiO_2 was obtained in the thermal CVD domain (position 2 in Fig. 3(a)), but no Kikuchi diffraction pattern was found in the thermal oxidation domain (position 1 in Fig. 3(a)). The comparison indicates that TCVD-SiO_2 tends to present distinct crystal features; however, TO-SiO_2 is certainly composed of amorphous SiO_2.

Table 1
Composition ratio of TO-SiO_2 and TCVD-SiO_2.

Oxidation			Peak Area	Sensitivity Factor	Composition Ratio (%)	
Thermal Oxidation (TO-SiO_2)	Si2p	Si^{4+}	3860	0.368	32.06	21.90
		Si^{3+}	7370		61.21	
		Si^{2+}	810		6.73	
	C1s	$Si_4C_{4-x}O_2$	2845	0.314	20.01	30.30
		Contaminant	6980		49.09	
		C-O	2676		18.82	
		C=O	1717		12.08	
	O1s	SiO_2	14200	0.733	27.13	47.80
		$Si_4C_{4-x}O_2$	18850		36.01	
		OH	19300		36.87	
Thermal CVD (TCVD-SiO_2)	Si2p	Si^{4+}	7500	0.368	54.66	24.76
		Si^{3+}	6070		44.24	
		Si^{2+}	150		1.09	
	C1s	$Si_4C_{4-x}O_2$	1133	0.314	14.09	17.00
		Contaminant	4251		52.88	
		C-O	1893		23.55	
		C=O	762		9.48	
	O1s	SiO_2	36100	0.733	56.14	58.24
		$Si_4C_{4-x}O_2$	17000		26.44	
		OH	11200		17.42	

Additionally, XPS was used to quantitatively analyze the atomic bonding conditions of TO-SiO_2 and TCVD-SiO_2. According to the peak area and sensitivity factor of each composition, we calculated the corresponding composition ratio based on the following equation

$$\left\{ \begin{array}{l} n_i = \dfrac{I_i}{S_i} \\ C_i = \dfrac{n_i}{\sum_i n_i} \end{array} \right. \quad (1)$$

where i represents the different compositions, including different

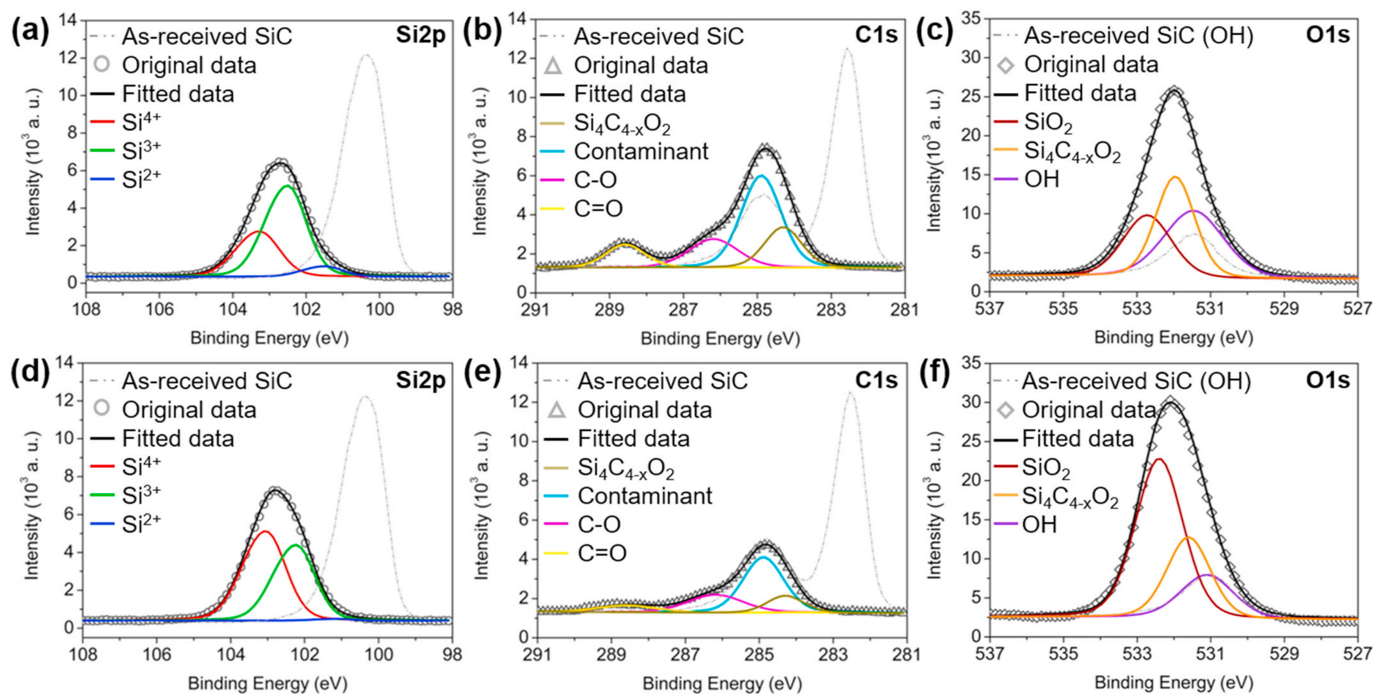

Fig. 4. XPS results of (a)–(c) TO-SiO_2 and (d)–(f) TCVD-SiO_2 on the heated 4H-SiC (1500 °C, 100 Pa, 10 min).

elements and valence states; I_i, S_i, and n_i are the peak area, sensitivity factor, and absolute content of composition i; C_i is the percentage composition of i. Table 1 summarizes the composition ratios of each element for one oxide and each bonding condition for one element. Considering the spin-orbit splitting, the Si2p spectra in Fig. 4(a) and (d) show different bonding features of Si in the two domains. The thermal oxidation domain contains two intermediate oxidation states (Si^{2+} and Si^{3+}) in addition to the eventual oxidation state (Si^{4+}) [34–36], and the composition ration of Si^{4+} is only 32.06%. However, the composition ratio of Si^{4+} in the thermal CVD domain is as high as 54.66%. For the C content in TO-SiO_2 and TCVD-SiO_2 (Fig. 4(b) and (e)) [37,38], the composition ratios are 30.30% and 17.00%, respectively. Because the oxidation layer is thinner in the thermal CVD domain than in the thermal oxidation domain (Fig. 5(e) and (h)), it is reasonable that C atoms in the thermal CVD domain are more easily diffused as a gaseous oxide. Hence, the total amount of C in TCVD-SiO_2 is less than that in TO-SiO_2, which means that the carbon-related byproducts in the former are less than that in the latter. As for the O1s spectra in Fig. 4(c) and (f) [39,40], the composition ratios of SiO_2 in TO-SiO_2 and TCVD-SiO_2 are 27.13% and 56.14%, respectively, while that of the intermediate oxide ($Si_4C_{4\text{-}x}O_2$, $x \leq 2$) are 36.01% and 26.44%, respectively. Significantly, the content of the final oxidation state of Si atoms in TCVD-SiO_2 is much higher than that in TO-SiO_2, and less carbon-related byproducts are generated during thermal CVD than thermal oxidation. Thus, combining with the morphology observation, Kikuchi diffraction pattern, and atomic bonding condition, it is concluded that the crystal quality of TCVD-SiO_2 is much better than that of TO-SiO_2.

3.3. Growth mechanisms of TO-SiO_2 and TCVD-SiO_2

To reveal the growth mechanisms of TO-SiO_2 and TCVD-SiO_2, we further studied the structure of SiC/TO-SiO_2 and SiC/TCVD-SiO_2 interfaces. Fig. 5(a) shows the original morphology of a SiC sample heated at 1500 °C and 100 Pa for 10 min. After etching by KOH at 550 °C for 15 s, the oxide layer was completely removed, accompanied by the emergence of some dislocations of SiC, which can be visualized as hexagonal etching pits in Fig. 5(b). More importantly, the etched thermal oxidation domain still seems to be very flat, and the radial-structured pattern has changed into a flower-shaped pattern comprised of countless pits. The detailed 3D topographies of these two interfaces are depicted in Fig. 5(c) and (d). The Sa roughness of the atomically flat SiC/TO-SiO_2 interface is only 0.27 nm; however, remarkable micron-sized pits are detected at the SiC/TCVD-SiO_2 interface.

TEM observations of SiC/TO-SiO_2 and SiC/TCVD-SiO_2 interfaces were shown in Fig. 5(e)-5(k). According to Fig. 5(e) and (h), the thickness of the TO-SiO_2 layer is approximately 400 nm, while the thickest part of the TCVD-SiO_2 layer is just around 230 nm, which indicates that the growth rate of the former is much faster than that of the latter. In addition, the atomic flatness of the SiC/TO-SiO_2 interface is verified in Fig. 5(f) and (g). By contrast, many micron-sized pits resulting from the sublimation of large quantities of Si atoms from SiC at 1500 °C exist at the SiC/TCVD-SiO_2 interface (Fig. 5(h)-5(k)). As shown in Fig. 5(j) and (k), the side face of the pit presents the distinct step-terrace structure, while its bottom face is extremely flat at the atomic scale. The two different interfaces provide significant evidence for the different growth mechanisms of SiO_2 in the two domains.

For the growth of TO-SiO_2, oxygen must diffuse to the interface, while the generated CO at the interface must diffuse out of the oxide layer. The shortest diffusion path exists between the protruding structure of the substrate and the flat surface of the oxide layer. Thus, protrusions on the SiC surface are more easily oxidized to TO-SiO_2, indicating that the thermal oxidation of SiC is conducted layer by layer. Therefore, it is rational that an atomically flat interface can be obtained after the formation of TO-SiO_2. With the decreasing of oxygen concentration, the effect of thermal oxidation is gradually weakened, while the sublimation process of Si atoms is enhanced accordingly. Some inherent defects of SiC become the first nucleation sites of TCVD-SiO_2. Since the Si atoms at the steps are easier than those at the terraces to sublimate from SiC due to the difference in the number of dangling bonds [41], these nucleation sites transversely expand as the thermal CVD process progresses, eventually forming the pits with step-terrace-structured side faces and flat bottom faces.

The difference in crystalline property between TO-SiO_2 and TCVD-SiO_2 can be attributed to the difference in surface mobility during the thermal oxidation (oxygen-rich) and thermal CVD (oxygen-poor)

Fig. 5. Morphologies of the SiC/TO-SiO_2 and SiC/TCVD-SiO_2 interfaces. (a) LSCM image of the 4H-SiC heated at 1500 °C and 100 Pa for 10 min. (b) LSCM image of the 4H-SiC in (a) after etching by KOH at 550 °C for 15 s. (c) and (d) AFM 3D morphology images of the thermal oxidation domain and thermal CVD domain after etching, respectively. (e)–(g) TEM images of the SiC/TO-SiO_2 interface. (h)–(k) TEM images of the SiC/TCVD-SiO_2 interface.

processes. Under the oxygen-rich condition, the thermal oxidation of SiC is conducted rapidly and an oxide layer is formed directly on SiC, which can be denoted as bulk growth. In this bulk growth, the first generated oxide is surrounded by molecules in the amorphous phase, and any molecule crossing the phase boundary can potentially join the following growth process [42]. Therefore, the corresponding surface mobility is low and the surface relaxation is insufficient, resulting in the formation of amorphous TO-SiO_2. Under the oxygen-poor condition, the sublimation of Si atoms and the formation, evolution, and adsorption of gaseous oxide are carried out on the SiC surface or in the ambient atmosphere, which can be regarded as surface growth. In this surface growth, the slow CVD rate leads to the high surface mobility and the sufficient surface relaxation, resulting in the growth of TCVD-SiO_2 with good crystal quality [42–44]. Overall, it is rational to conclude that the different growth modes and the resulting different surface mobility determine the differences in morphology and crystal quality between TO-SiO_2 and TCVD-SiO_2.

3.4. Epitaxial growth of graphene on the SiC substrate

To further explore the role of oxygen in the surface kinetics of single crystal SiC, we conducted the heat treatment of SiC at approximately 1.0×10^{-3} Pa, which means that the corresponding oxygen concentration is about one ten millionth of that at 1 atm. After the treatment at 1500 °C for 10 min, graphene was formed on SiC owing to the extensive sublimation of Si atoms, the rearrangement of C atoms, and the almost

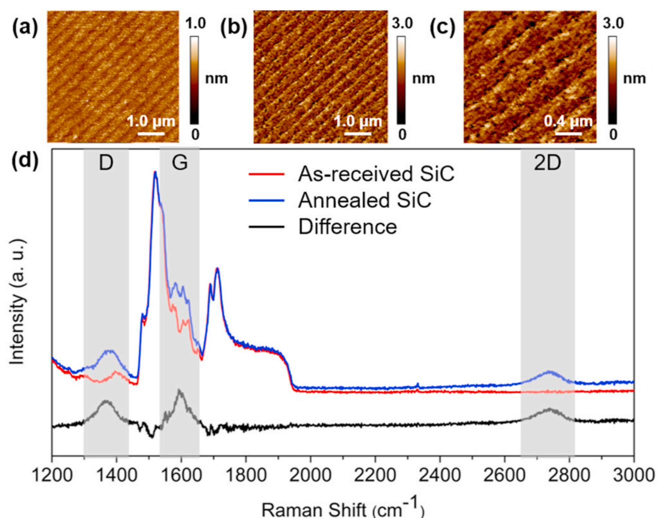

Fig. 6. AFM images of (a) as-received 4H-SiC and (b, c) heated 4H-SiC (1500 °C, $\sim 1.0 \times 10^{-3}$ Pa, 10 min). (d) Raman spectrum of graphene formed on the heated 4H-SiC.

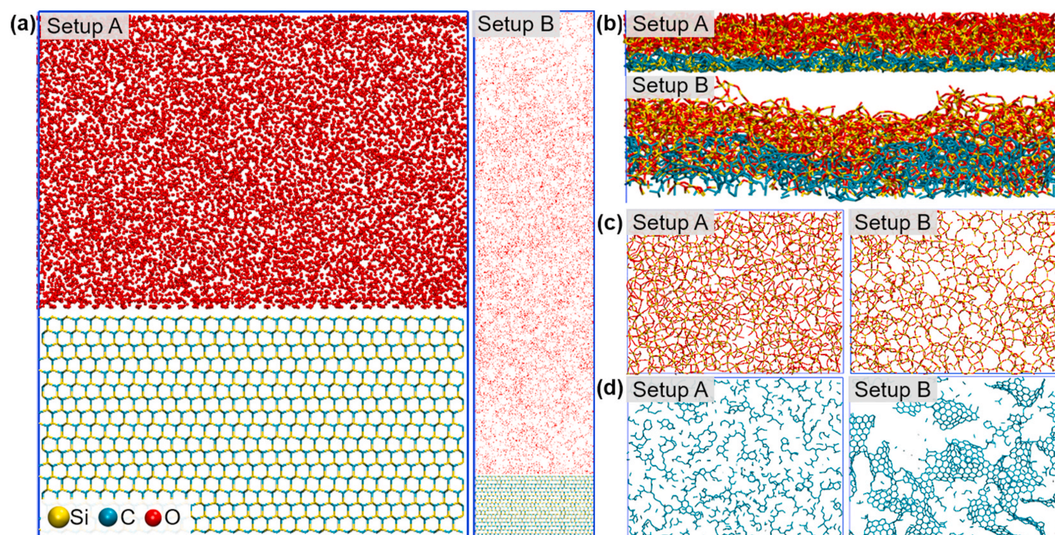

Fig. 7. Simulation setups and results. (a) Two molecular dynamics simulation setups used in our study. (b) Configurations of the reaction layers in Setup A and Setup B after equilibrium (5 ns). (c) and (d) Top view of the generated oxide layer and carbon buffer layer in Setup A and Setup B after equilibrium (5 ns), respectively.

oxygen-free reaction atmosphere [16]. Fig. 6(a)–6(c) show the AFM images of the as-received and annealed SiC. By subtracting the Raman spectrum of as-received SiC from that of annealed SiC, we obtained the Raman spectrum of graphene, which was labeled as 'Difference' in Fig. 6 (d). Clearly, the G and 2D signals together with a defect D peak indicate that graphene with defects was formed on the SiC substrate after the annealing treatment. Thus, it is concluded that when the oxygen concentration drops to an extremely low value, neither TO-SiO_2 nor TCVD-SiO_2 grows on SiC; however, graphene is formed because the C atoms remaining on the surface cannot be oxidized after the sublimation of Si atoms in an almost oxygen-free reaction atmosphere.

3.5. ReaxFF reactive molecular dynamics simulation

A molecular dynamics simulation based on the ReaxFF force field was used to further illustrate the role of oxygen in the surface kinetics of SiO_2 growth on single crystal SiC at elevated temperatures. As an empirical bond-order-dependent potential, the ReaxFF method allows for fully reactive atom-scale molecular dynamics of chemical reactions and has been widely used for the study on the oxidation of Si and SiC [45–47]. To apply the ReaxFF method to our simulation system with Si, O, and C elements, we combined the corresponding potential functions (Tersoff potential and Lennard-Jones potential) of these three elements to facilitate the analysis of the bonding conditions of Si-C, Si-O, and C-C (Supplementary Information Note 1 and Tables S1–S3). To confirm the accuracy and rationality of our simulation results, the binding energy of oxygen absorbed at different site positions on the SiC surface was first calculated by the quantum mechanics (QM) method and the ReaxFF method, respectively (Supplementary Information Note 2 and Fig. S1). It is clear that the binding energy values calculated by these two methods are numerically close to each other. Additionally, the bond lengths of C-Si, O-Si, and C-C were calculated based on the related radial distribution function (RDF) curves, and these calculated values are numerically close to the corresponding theoretical values, further ensuring the validity of our simulation results (Supplementary Information Note 2, Fig. S2, and Table S4). Moreover, the changes in the binding energy of three small setups containing one Si atom and one C atom, six Si atoms and six C atoms, and six C atoms, respectively, were studied with the evolution of structures, which can account for the formation of specific configurations in our simulation setups (Supplementary Information Note 3 and Fig. S3).

We established two simulation setups (Setup A and Setup B), as shown in Fig. 7(a). The two setups contain the same number of C, O, and Si atoms, but the volume of Setup B is approximately three times larger than that of Setup A. Thus, Setup A can be regarded as an oxygen-rich reaction setup, while Setup B is an oxygen-poor reaction setup. The temperature in both setups is set to 1800 K, which is closed to the temperature in the oxidation experiments. Fig. 7(b) shows the final configurations of the reaction layers in Setup A and Setup B after the simulation processes reached equilibrium, and Fig. 7(c) and (d) show details of the typical oxide layer and carbon buffer layer of the two setups from the top view, respectively. In contrast, a compact oxide layer with a disordered atomic arrangement was formed on the SiC substrate in Setup A, while the oxide layer in Setup B seems to be porous, and some regular Si-O rings can be observed. Moreover, the carbon buffer layer in Setup A also shows disordered features, while the buffer layer in Setup B tends to form a graphene-like structure. All these differences are attributed to the differences in oxygen concentrations. Specifically, in an oxygen-rich reaction setup, the thermal oxidation of SiC occurs relatively fast, and the generated SiO_2 and residual C atoms are promptly adsorbed into the adjacent sites rather than the best adsorption site because this process may be under non-thermodynamic equilibrium conditions, thus forming the amorphous TO-SiO_2 layer and the disordered carbon buffer layer. However, in an oxygen-poor reaction setup, the aforementioned reaction occurs to a lesser extent than in an oxygen-rich reaction setup, and the sublimated Si atoms can easily eliminate the restriction of the thin oxide layer, and form Si_xO_y with active oxygen in the gas phase. Consequently, the generated gaseous oxide is adsorbed onto the preferred sites on the SiC substrate owing to the CVD process being at thermodynamic equilibrium. The nucleation sites of the radial-structured patterns resulting from the growth of TCVD-SiO_2 may be related to the inherent defects of the substrate (Supplementary Information Note 4 and Fig. S4). Moreover, C atoms on the substrate surface can also seek the preferred adsorption sites and ultimately form stable graphene-like structures.

Additionally, each bond type, cluster type, and ring type from the molecular dynamic simulation trajectories of Setup A and Setup B were identified and counted. As shown in Fig. 8(a), Si-O and C-C bonds were formed at the expense of Si-C bonds in both setups. For the three-atom clusters in Fig. 8(b), the species considered are C-Si-C (SiC), O-Si-O (SiO_2), and C-C-C (carbonaceous material), each of which represents the composite species in parentheses that may form and/or disappear during the reaction. It is clear that C-Si-C species were rapidly consumed, while O-Si-O and C-C-C species were consequently formed in the two

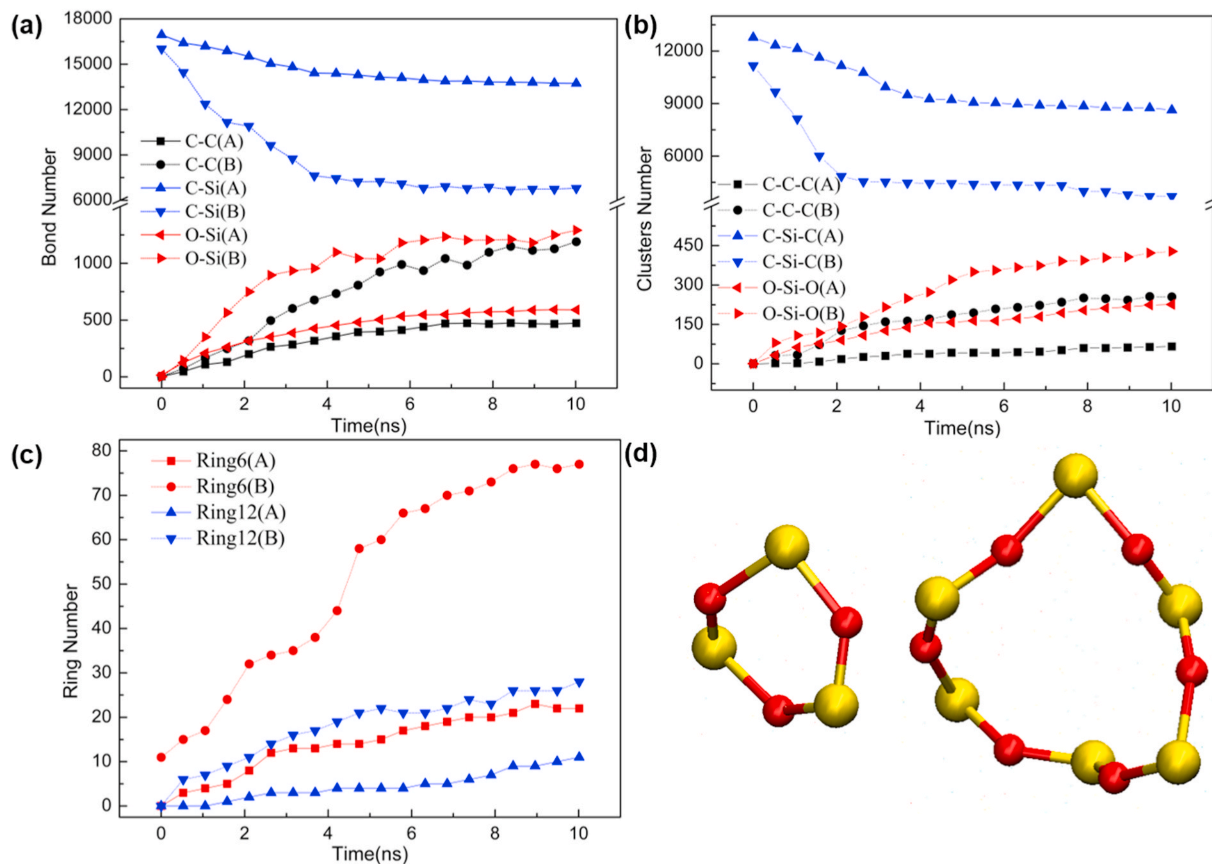

Fig. 8. Quantity changes of the (a) bonds, (b) clusters, and (c) six-membered and twelve-membered rings composed of Si and O atoms in Setup A and Setup B during the simulations. (d) The typical six-membered and twelve-membered rings in the simulations.

setups. More importantly, the number of both O-Si-O and C-C-C species in Setup B is greater than that in Setup A, which is consistent with the results in Fig. 7(b)-7(d). According to the crystal structure of single crystal SiO_2, the arrangement of Si and O atoms can present a six-membered or twelve-membered ring structure. Hence, we counted the number of six-membered and twelve-membered ring structures in the two setups, and the results can be used as a rough criterion to qualitatively judge the crystal quality of SiO_2. Fig. 7(d) shows the typical six-membered and twelve-membered ring structures obtained in our simulations. As shown in Fig. 7(c), more six-membered and twelve-membered rings were formed in Setup B than in Setup A. Thus, it can be inferred that the oxide layer in Setup B is more likely than that in Setup A to form an ordered structure.

Fig. 9(a) and (b) show the structural evolutions of the two setups in the simulation, respectively. The oxidation of SiC in Setup A was conducted layer by layer as oxygen rapidly diffused to the interface, resulting in an oxide layer with a flat surface and a flat SiC/SiO_2 interface. The above oxidation process demonstrates the growth of TO-SiO_2. SiC in Setup B, however, underwent a completely different oxidation process. Fig. 9(c) shows not only the diffusion and adsorption of oxygen (the formation process of TO-SiO_2) but also the sublimation of Si atoms, and the formation, evolution and adsorption of gaseous Si_xO_y (the growth process of TO-SiO_2) in Setup B. The results verify the different oxidation mechanisms of SiC at the atomic scale in the oxygen-rich and oxygen-poor setups. Thus, it is confirmed that the decrease in oxygen concentration can promote the growth kinetics of SiO_2 on single crystal SiC from being dominated by thermal oxidation to being dominated by thermal CVD.

4. Conclusions

In this paper, we comprehensively investigate the role of oxygen in manipulating the surface kinetics of SiO_2 growth on single crystal SiC at elevated temperatures based on the experiments and ReaxFF reactive molecular dynamics simulation. Our work clearly reveals that oxygen concentration can strongly affect the domain morphology, crystal quality, interface structure, and growth kinetics of SiO_2 on the SiC substrate. To summarize, the main conclusions are given below:

(1) Oxygen concentration determines the competitive growth of TO-SiO_2 and TCVD-SiO_2 on the SiC substrate at 1500 °C. We experimentally and theoretically reveal that the decrease in oxygen concentration can promote the growth kinetics of SiO_2 on SiC from being dominated by thermal oxidation to being dominated by thermal CVD.
(2) We demonstrate that the crystal quality of TCVD-SiO_2 is much better than that of TO-SiO_2, which may open the door to grow the high-quality oxide layer for fabricating high-performance SiC-based electronic devices only by controlling the oxygen concentration in the reaction system.
(3) The layer-by-layer oxidation mechanism and the SiC atomic steps transverse evolution mechanism are proposed for TO-SiO_2 growth and TCVD-SiO_2 growth at the atomic scale, respectively.

Declaration of competing interest

The authors declare that they have no known competing financial interests or personal relationships that could have appeared to influence the work reported in this paper.

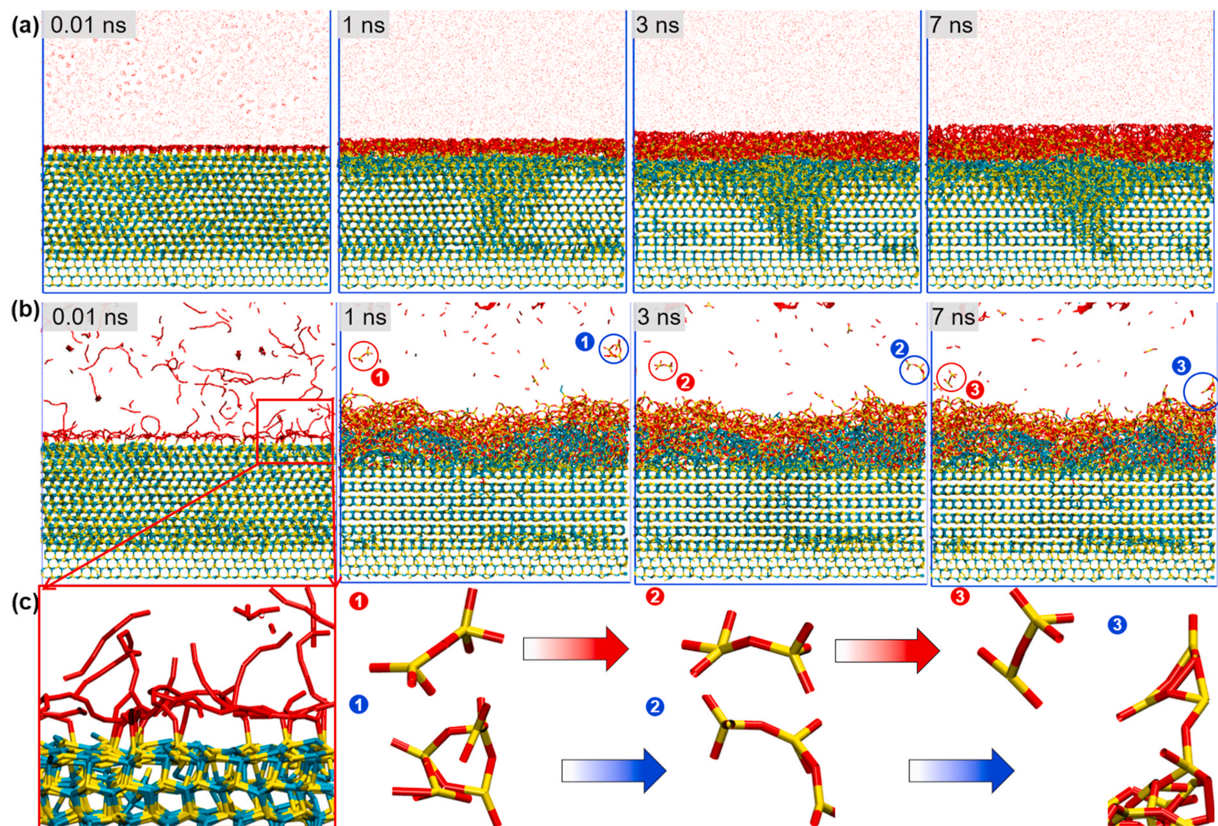

Fig. 9. Detailed evolutions of the simulation setups. (a) and (b) Structural evolutions of Setup A and Setup B during the simulations. (c) The diffusion and adsorption of oxygen, and the formation, evolution and adsorption of gaseous Si_xO_y in Setup B.

Acknowledgments

This work was financially supported by the research fund for International Cooperation (GJHZ20180928155412525) and the Shenzhen High-level Innovation and Entrepreneurship Fund (No. KQTD20170810110250357) from the Science and Technology Innovation Committee of Shenzhen Municipality, Shenzhen, China. The authors acknowledge the assistance of SUSTech Core Research Facilities.

Appendix A. Supplementary data

Supplementary data to this article can be found online at https://doi.org/10.1016/j.ceramint.2020.09.014.

References

[1] M. Bhatnagar, B.J. Baliga, Comparison of 6H-SiC, 3C-SiC, and Si for power devices, IEEE Trans. Electron. Dev. 40 (1993) 645–655.
[2] D. Nakamura, I. Gunjishima, S. Yamaguchi, T. Ito, A. Okamoto, H. Kondo, S. Onda, K. Takatori, Ultrahigh-quality silicon carbide single crystals, Nature 430 (2004) 1009–1012.
[3] W. Wondrak, R. Held, E. Niemann, U. Schmid, SiC devices for advanced power and high-temperature applications, IEEE Trans. Ind. Electron. 48 (2001) 307–308.
[4] H.-P. Phan, Y. Zhong, T.-K. Nguyen, Y. Park, T. Dinh, E. Song, R.K. Vadivelu, M. K. Masud, J. Li, M.J.A. Shiddiky, D. Dao, Y. Yamauchi, J.A. Rogers, N.-T. Nguyen, Transferred crystalline silicon carbide nanomembranes for implantable flexible electronics, ACS Nano 13 (2019) 11572–11581.
[5] K. Daviau, K.K.M. Lee, High-pressure, high-temperature behavior of silicon carbide: a review, Crystals 8 (2018) 217.
[6] S. Zheng, Z. Li, Z.-S. Wu, Y. Dong, F. Zhou, S. Wang, Q. Fu, C. Sun, L. Guo, X. Bao, High packing density unidirectional arrays of vertically aligned graphene with enhanced areal capacitance for high-power micro-supercapacitors, ACS Nano 11 (2017) 4009–4016.
[7] K. Fukuda, M. Kato, K. Kojima, J. Senzaki, Effect of gate oxidation method on electrical properties of metal-oxide-semiconductor field-effect transistors fabricated on 4H-SiC C(000$\bar{1}$) face, Appl. Phys. Lett. 84 (2004) 2088–2090.
[8] Y.-M. Lin, C. Dimitrakopoulos, K.A. Jenkins, D.B. Farmer, H.-Y. Chiu, A. Grill, Ph Avouris, 100-GHz transistors from wafer-scale epitaxial graphene, Science 327 (2010) 662.
[9] Y. Song, S. Dhar, L.C. Feldman, G. Chung, J.R. Williams, Modified Deal Grove model for the thermal oxidation of silicon carbide, J. Appl. Phys. 95 (2004) 4953–4957.
[10] R.H. Kikuchi, K. Kita, Fabrication of SiO_2/4H-SiC (0001) interface with nearly ideal capacitance-voltage characteristics by thermal oxidation, Appl. Phys. Lett. 105 (2014), 032106.
[11] S. Dhar, L.C. Feldman, S. Wang, T. Isaacs-Smith, J.R. Williams, Interface trap passivation for SiO_2/(000$\bar{1}$) C-terminated 4H-SiC, J. Appl. Phys. 98 (2005), 014902.
[12] H. Kurimoto, K. Shibata, C. Kimura, H. Aoki, T. Sugino, Thermal oxidation temperature dependence of 4H-SiC MOS interface, Appl. Surf. Sci. 253 (2006) 2416–2420.
[13] K.S. Novoselov, A.K. Geim, S.V. Morozov, D. Jiang, Y. Zhang, S.V. Dubonos, I. V. Grigorieva, A.A. Firsov, Electric field effect in atomically thin carbon films, Science 306 (2004) 666–669.
[14] S. Park, J. An, J.R. Potts, A. Velamakanni, S. Murali, S.R. Ruoff, Hydrazine-reduction of graphite- and graphene oxide, Carbon 49 (2011) 3019–3023.
[15] S. Bae, H. Kim, Y. Lee, X. Xu, J.-S. Park, Y. Zheng, J. Balakrishnan, T. Lei, H.R. Kim, Y.I. Song, Y.-J. Kim, K.S. Kim, B. Ozyilmaz, J.-H. Ahn, B.-H. Hong, S. Iijima, Roll-to-roll production of 30-inch graphene films for transparent electrodes, Nat. Nanotechnol. 5 (2010) 574–578.
[16] K.V. Emtsev, A. Bostwick, K. Horn, J. Jobst, G.L. Kellogg, L. Ley, J.L. McChesney, T. Ohta, S.A. Reshanov, J. Rohrl, E. Rotenberg, A.K. Schmid, D. Waldmann, H. B. Weber, T. Seyller, Towards wafer-size graphene layers by atmospheric pressure graphitization of silicon carbide, Nat. Mater. 8 (2009) 203–207.
[17] V. Yu Aristov, G. Urbanik, K. Kummer, D.V. Vyalikh, O.V. Molodtsova, A. B. Preobrajenski, A.A. Zakharov, C. Hess, T. Hanke, B. Buchner, I. Vobornik, J. Fujii, G. Panaccione, Y.A. Ossipyan, M. Knupfer, Graphene synthesis on cubic SiC/Si wafers. Perspectives for mass production of graphene-based electronic devices, Nano Lett. 10 (2010) 992–995.
[18] Y. Hao, M.S. Bharathi, L. Wang, Y. Liu, H. Chen, S. Nie, X. Wang, H. Chou, C. Tan, B. Fallahazad, H. Ramanarayan, C.W. Magnuson, E. Tutuc, B.I. Yakobson, K. F. McCarty, Y.-W. Zhang, P. Kim, J. Hone, L. Colombo, R.S. Ruoff, The role of surface oxygen in the growth of large single-crystal graphene on copper, Science 342 (2013) 720–723.
[19] T.A. Witten Jr., L.M. Sander, Diffusion-limited aggregation, a kinetic critical phenomenon, Phys. Rev. Lett. 47 (1981) 1400–1403.

[20] J. Li, M. Chen, C. Zhang, H. Dong, W. Lin, P. Zhuang, Y. Wen, B. Tian, W. Cai, X. Zhang, Fractal-theory-based control of the shape and quality of CVD-grown 2D materials, Adv. Mater. 31 (2019) 1902431.

[21] X. Li, S. Zhang, S. Chen, X. Zhang, J. Gao, Y.-W. Zhang, J. Zhao, X. Shen, R. Yu, Y. Yang, L. He, J. Nie, C. Xiong, R. Dou, Mo concentration controls the morphological transitions from dendritic to semicompact, and to compact growth of monolayer crystalline MoS_2 on various substrates, ACS Appl. Mater. Interfaces 11 (2019) 42751–42759.

[22] I. Vlassiouk, M. Regmi, P. Fulvio, S. Dai, P. Datskos, G. Eres, S. Smirnov, Role of hydrogen in chemical vapor deposition growth of large single-crystal graphene, ACS Nano 5 (2011) 6069–6076.

[23] Y. Liu, S. Bhowmick, B.I. Yakobson, BN white graphene with "colorful" edges: the energies and morphology, Nano Lett. 11 (2011) 3113–3116.

[24] V.I. Artyukhov, Y. Liu, B.I. Yakobson, Equilibrium at the edge and atomistic mechanisms of graphene growth, Proc. Natl. Acad. Sci. U.S.A. 109 (2012) 15136–15140.

[25] E. Meca, J. Lowengrub, H. Kim, C. Mattevi, V.B. Shenoy, Epitaxial graphene growth and shape dynamics on copper: phase-field modeling and experiments, Nano Lett. 13 (2013) 5692–5697.

[26] H. Deng, N. Liu, K. Endo, K. Yamamura, Atomic-scale finishing of carbon face of single crystal SiC by combination of thermal oxidation pretreatment and slurry polishing, Appl. Surf. Sci. 434 (2018) 40–48.

[27] H. Deng, K. Endo, K. Yamamura, Atomic-scale planarization of 4H-SiC (0001) by combination of thermal oxidation and abrasive polishing, Appl. Phys. Lett. 103 (2013) 111603.

[28] R.L. Penn, J.F. Banfield, Imperfect oriented attachment: dislocation generation in defect-free nanocrystals, Science 281 (1998) 969–971.

[29] K. Shibata, K. Taniguchi, Generation mechanism of dislocations in local oxidation of silicon, J. Electrochem. Soc. 127 (1980) 1383–1387.

[30] E.P. EerNisse, Stress in thermal SiO_2 during growth, Appl. Phys. Lett. 35 (1979) 8–10.

[31] K. Chokawa, M. Araidai, K. Shiraishi, Effects of annealing with CO and CO_2 molecules on oxygen vacancy defect density in amorphous SiO_2 formed by thermal oxidation of SiC, J. Appl. Phys. 124 (2018) 135701.

[32] S. Nishikawa, S. Kikuchi, Diffraction of cathode rays by calcite, Nature 122 (1928), 726-726.

[33] P.W. Trimby, Y. Cao, Z. Chen, S. Han, K.J. Hemker, J. Lian, X. Liao, P. Rottmann, S. Samudrala, J. Sun, J.T. Wang, J. Wheeler, J.M. Cairney, Characterizing deformed ultrafine-grained and nanocrystalline materials using transmission Kikuchi diffraction in a scanning electron microscope, Acta Mater. 62 (2014) 69–80.

[34] F.J. Himpsel, F.R. McFeely, A. Taleb-Ibrahimi, J.A. Yarmoff, G. Hollinger, Microscopic structure of the SiO_2/Si interface, Phys. Rev. B 38 (1988) 6084–6096.

[35] N. Saito, D. Mori, A. Imafuku, K. Nishitani, H. Sakane, K. Kawai, Y. Sano, M. Morita, K. Arima, Aggregation of carbon atoms at SiO_2/SiC(0001) interface by plasma oxidation toward formation of pit-free graphene, Carbon 80 (2014) 440–445.

[36] N. Koshizaki, H. Umehara, T. Oyama, XPS characterization and optical properties of Si/SiO_2, Si/Al_2O_3 and Si/MgO co-sputtered films, Thin Solid Films 325 (1998) 130–136.

[37] B. Hornetz, H.-J. Michel, J. Halbritter, Oxidation and 6H-SiC–SiO_2 interfaces, J. Vac. Sci. Technol., A 13 (1995) 767–771.

[38] H. Watanabe, T. Hosoi, T. Kirino, Y. Kagei, Y. Uenishi, A. Chanthaphan, A. Yoshigoe, Y. Teraoka, T. Shimura, Synchrotron x-ray photoelectron spectroscopy study on thermally grown SiO_2/4H-SiC(0001) interface and its correlation with electrical properties, Appl. Phys. Lett. 99 (2011), 021907.

[39] K. Yamamura, T. Takiguchi, M. Ueda, H. Deng, A.N. Hattori, N. Zettsu, Plasma assisted polishing of single crystal SiC for obtaining atomically flat strain-free surface CIRP, Ann.-Manuf. Techn. 60 (2011) 571–574.

[40] H. Deng, T. Takiguchi, M. Ueda, A.N. Hattori, N. Zettsu, K. Yamamura, Damage-free dry polishing of 4H-SiC combined with atmospheric-pressure water vapor plasma oxidation, Jpn. J. Appl. Phys. 50 (2011), 08JG05.

[41] W. Li, J. Zhao, Q. Zhu, D. Wang, Oxidation of step edges on vicinal 4H-SiC(0001) surfaces, Appl. Phys. Lett. 103 (2013) 211603.

[42] C.W. Brian, L. Yu, Surface self-diffusion of organic glasses, J. Phys. Chem. 117 (2013) 13303–13309.

[43] S.F. Swallen, K.L. Kearns, M.K. Mapes, Y.S. Kim, R.J. McMahon, M.D. Ediger, T. Wu, L. Yu, S. Satija, Organic glasses with exceptional thermodynamic and kinetic stability, Science 315 (2007) 353–356.

[44] C.R. Cao, Y.M. Lu, H.Y. Bai, W.H. Wang, High surface mobility and fast surface enhanced crystallization of metallic glass, Appl. Phys. Lett. 107 (2015) 141606.

[45] T.P. Senftle, S. Hong, M.M. Islam, S.B. Kylasa, Y. Zheng, Y.K. Shin, C. Junkermeier, R. Engel-Herbert, M.J. Janik, H.M. Aktulga, T. Verstraelen, A. Grama, A.C.T. van Duin, The ReaxFF reactive force-field: development, applications and future directions, npj Comput. Mater. 2 (2016) 15011.

[46] D.A. Newsome, D. Sengupta, H. Foroutan, M.F. Russo, A.C.T. van Duin, Oxidation of silicon carbide by O_2 and H_2O: a ReaxFF reactive molecular dynamics study, Part I, J. Phys. Chem. C 116 (2012) 16111–16121.

[47] A.C.T. van Duin, A. Strachan, S. Stewman, Q. Zhang, X. Xu, W.A. Goddard III, $ReaxFF_{SiO}$ reactive force field for silicon and silicon oxide systems, J. Phys. Chem. 107 (2003) 3803–3811.